Oxidative Dehydrogenation of Propane by Monomeric Vanadium Oxide Sites on Silica Support

Xavier Rozanska, Rémy Fortrie, and Joachim Sauer*

Institut für Chemie, Humboldt Universität zu Berlin, Unter den Linden 6, D-10099 Berlin, Germany

Received: February 19, 2007

We investigate possible mechanisms of oxidative dehydrogenation of propane using density functional theory. Monomeric vanadium oxide species supported on silica are modeled by vanadyl-substituted silsesquioxane. Similarly to other catalysts with transition metal oxo bonds, the initial C−H bond activation step is hydrogen abstraction by the vanadyl ($O{=}V^{V}$) group yielding a diradical intermediate in which a propyl radical is bound to a $HO-V^{IV}$ site. This is followed by a propyl rebound mechanism yielding alkoxide or alcohol attached to a $V^{III}(OSi)_3$ surface site from which propene can be formed. Propene is also directly obtained by a second hydrogen abstraction from the diradical intermediate. Desorption of propyl radicals leads to a stationary concentration of propyl in the gas phase and leaves reduced $HO-V^{IV}$ sites on the surface. Due to fast reoxidation their concentration is much smaller than the concentration of $O{=}V^{V}$ sites. Therefore the rate of propene formation after readsorption on $O{=}V^{V}$ sites is much larger than the rate of isopropyl alcohol (or propene) formation after readsorption on $HO-V^{IV}$ sites. Generation of surface propyl radicals by the first hydrogen abstraction becomes rate limiting. We predict that at 750 K the apparent activation energy is 123 ± 5 kJ/mol and the rate constant is about 0.26 s^{-1}, in close agreement with experiments. The first hydrogen abstraction occurs exclusively on $O{=}V^{V}$ sites, while the second hydrogen abstraction can also occur on V−O−Si bridging oxygen sites.

1. Introduction

The catalytic activation of C−H bonds is of fundamental interest, because it is the crucial step in important technological processes and also in many enzymatic reactions. Examples are the oxidative dehydrogenation (ODH) of lower alkanes to alkenes by, for example, supported transiton metal oxide catalysts[1,2] and the oxygenation of C−H bonds to C−OH groups by cytochrom P450.[3] For transition metal oxide species there is experimental and computational evidence that the initial C−H activation is hydrogen abstraction by metal oxo bonds,[4]

$$R-H + O{=}M(d^{n}) \rightarrow R^{\bullet} + HO-M(d^{n+1}) \qquad (1)$$

with d^n denoting the occupation of nonbonding d-states on vanadium. The alkyl radical can directly form alkenes by losing another hydrogen atom,[5] but it can also form an alcohol by a rebound mechanism as suggested for enzyme P450, see, e.g., ref 3 and references therein:

$$R^{\bullet} + HO-M(d^{n+1}) \rightarrow H(R)O{\cdot}M(d^{n+2}) \qquad (2)$$

From the alcohol intermediate, an alkene can be obtained by elimination.

Alternative mechanisms suggest oxidative addition of the C−H bond onto the O═M bond as the initial step according to:[6]

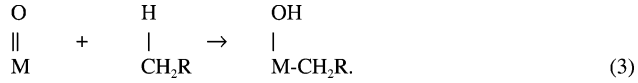

(3)

Fu et al.[7] have considered many possible initial steps for the activation of propane by Mo_3O_9. Hydrogen abstraction turned out to have the lowest barrier. Previous quantum chemical studies have considered the oxidative dehydrogenation of propane by bulk V_2O_5.[8,9] Gas-phase reactions of propane with VO_2^+ and $V_3O_7^+$ have also been analyzed.[10,11]

We examine possible reaction mechanisms for the oxidative dehydrogenation of propane by supported transition metal oxide catalysts. Specifically we are interested in V_2O_5 supported on SiO_2[2,12,13] and consider monomeric $O{=}V(O-)_3$ surface species,

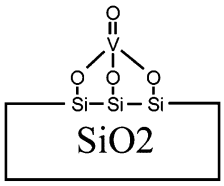

which together with dimeric and oligomeric V_2O_5 species are present on catalyst surfaces with low V_2O_5 loadings.[13] In the oxidative dehydrogenation of propane by monomeric sites,

$$C_3H_8 + O{=}V(O-)_3 \rightarrow C_3H_6 + H_2O{\cdot}V(O-)_3 \qquad (4)$$

vanadium is reduced from $V^{V}(d^0)$ to $V^{III}(d^2)$. At the same time, the spin state changes from singlet to triplet. We do not consider the full catalytic cycle. The oxidation of the substrate can be

* Address correspondence to this author. E-mail: js@chemie.hu-berlin.de.

10.1021/jp071409e CCC: $37.00
Published on Web 03/30/2007

kinetically separated from reoxidation of the catalyst, which is not the rate determining step in the oxidative dehydrogenation of alkane.[14,15]

2. Models and Methods

To model monomeric vanadium oxide species on silicon oxide we use the cubic silsesquioxane $H_8Si_8O_{12}$ in which one Si−H group is replaced by a vanadyl group. This model has

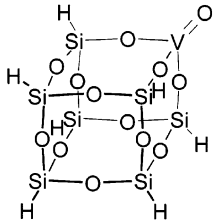

proven useful in previous studies.[16,17] $H_8Si_8O_{12}$ mimics well the electronic structure of silica and is also sufficiently flexible to realistically simulate structural relaxations at reaction sites.[18−21]

We apply density functional theory (DFT) with the hybrid B3LYP functional[22] and triple-ζ plus polarization (TZVP) basis sets on all atoms[23] and employ Turbomole 5.7.[24] B3LYP gives vanadium oxide reduction energies in good agreement with more accurate quantum chemical methods and the few experimental results available.[25] The optimized structures are characterized as minima or saddle points by frequency calculations. All reported energies are zero-point corrected unless otherwise stated. Finite temperature contributions to enthalpies and Gibbs free energies are estimated within the rigid rotor−harmonic oscillator−ideal gas approximation.

Unrestricted Kohn−Sham (UB3LYP) is used for triplet or doublet spin state systems. Broken-symmetry calculations are performed for open-shell singlets.[26] In this approach, the energy of the low spin state (E_{ls}) is obtained by spin projection from the energies of the broken-symmetry (E_{bs}) solution and the triplet (E_{tr}^{spe}) solution for a given geometric structure:[27]

$$E_{ls} = \frac{2E_{bs} - \langle S^2\rangle_{bs} E_{tr}^{spe}}{2 - \langle S^2\rangle_{bs}} \tag{5}$$

$\langle S^2\rangle_{bs}$ is the expectation value of the total-spin operator value for the broken-symmetry solution. $\langle S^2\rangle_{bs}$ is equal to one in the ideal case of non-interacting spins in equivalent orbitals. For cases in which $\langle S^2\rangle_{bs}$ significantly deviates from one, spin-projection has been questioned,[28] and E_{bs} should be taken as the upper limit estimate. Zero-point vibrational energy corrections are calculated for the broken-symmetry potential energy surface and, where appropriate, added to the spin-projected energy.

Classical transition state theory is used to calculate intrinsic rate constants, k,

$$k = \frac{k_B T}{h} \exp\left(-\frac{G_{Ts} - G_{Int}}{RT}\right) = \frac{k_B T}{h} \frac{q_{Ts}}{q_{Int}} \exp\left(-\frac{E_{ZP}^{Ts} - E_{ZP}^{Int}}{RT}\right) \tag{6a}$$

and apparent rate constants, k_{app},

$$k_{app} = K{\cdot}k = \frac{k_B T}{h} \exp\left(-\frac{G_{Ts} - G_{S+hc}}{RT}\right) = \frac{k_B T}{h} \frac{q_{Ts}}{q_S{\cdot}q_{hc}} e \exp\left(-\frac{E_{ZP}^{Ts} - E_{ZP}^{S+hc}}{RT}\right) \tag{6b}$$

with G and E_{ZP} being the Gibbs free energies and the zero-point energies, respectively, of transition structures (Ts), intermediates (Int), and hydrocarbon species in the gas phase separated from surface sites (S+hc). K is the equilibrium constant for formation of the intermediate Int from S+hc. The partition functions for the gas-phase species are calculated within the harmonic oscillator−rigid rotor−ideal gas approximation including vibrational, rotational, and translational degrees of freedom. As part of a solid body, the surface species Ts, Int, and S do not have rotational or translational degrees of freedom. All $N - 6$ internal degrees of freedom, including internal hindered rotations, are treated as harmonic vibrations. Low frequencies (in cm^{-1} in parentheses) are encountered for intermediates in which hydrocarbon species are weakly bound to the surface site: Int1 (3.2, 5.6), Int3(tr) (7.7), Int3(bs) (6.1), Ts7 (6.1, 5.9), and Ts13 (8.8). An error of 3 cm^{-1} on a wavenumber of 5 cm^{-1} and another error of 3 cm^{-1} on a wavenumber of 10 cm^{-1} cause a combined error of 3, 9, and 12 kJ/mol at 200, 600, and 800 K. We may take these as estimates of the uncertainty of our calculated Gibbs free energy values.

3. Results

3.1. Reaction Mechanisms on Isolated Sites. Figure 1 shows the different reaction routes for the oxidative dehydrogenation of propane at an isolated vanadium oxide site on the silica surface. Figures 2 and 3 show the geometric details of the intermediates and transition structures, respectively. The corresponding energies are reported in Table 1.

The first step is adsorption of propane onto the surface site leading to the van der Waals complex Int1. As other widely used functionals, B3LYP poorly describes dispersion, which is the major stabilizing contribution in van der Waals complexes.[29,30] This explains the apparent absence of binding between propane and the surface site model. The enthalpy of adsorption of propane onto V_2O_5 at 298 K is 37 ± 5 kJ/mol,[31] which constitutes a realistic estimate of the binding in Int1.

From Int1, two reaction routes can be followed, namely hydrogen abstraction by the oxygen atom of the vanadyl group through Ts1 or by one of the three bridging V−O−Si oxygen atoms through Ts2. Which oxygen atom is involved in the activation of the first carbon−hydrogen bond is a question that has been frequently raised in the literature,[9,12,15,32] but never unambiguously answered for supported transition metal oxide species. The products after Ts1 and Ts2, Int2 and Int3, respectively, are biradicals in which a propyl radical weakly interacts with a $HO-V^{IV}(d^1)$ site. Dissociation of $C_3H_7^{\bullet}$ from the $HO-V^{IV}(d^1)$ site requires only 15 and 24 kJ/mol, respectively. The broken symmetry solution yields an energy within 1 kJ/mol of the triplet calculation, which implies that singlet and triplet states are almost degenerate.

The transition structures Ts1 and Ts2 are found only on the broken-symmetry surface. The energy barriers are 144 and 204 kJ/mol, respectively. After spin-projection, these values are 27 and 12 kJ/mol lower, respectively. The intermediates Int2 and Int3 are only 12 and 24 kJ/mol below the respective transition structures, which points to the "late" nature of the latter. Because Ts2 is 60 kJ/mol above Ts1 only the vanadyl group will be involved in the initial activation of propane. Consideration of the free energies of Ts1 and Ts2 at different temperatures (Table 1) does not change the dominance of the route through Ts1.

Different consecutive reaction steps toward propene formation can take place from Int2 and Int3 and all transition structures have triplet electronic states. For some of them, the existence

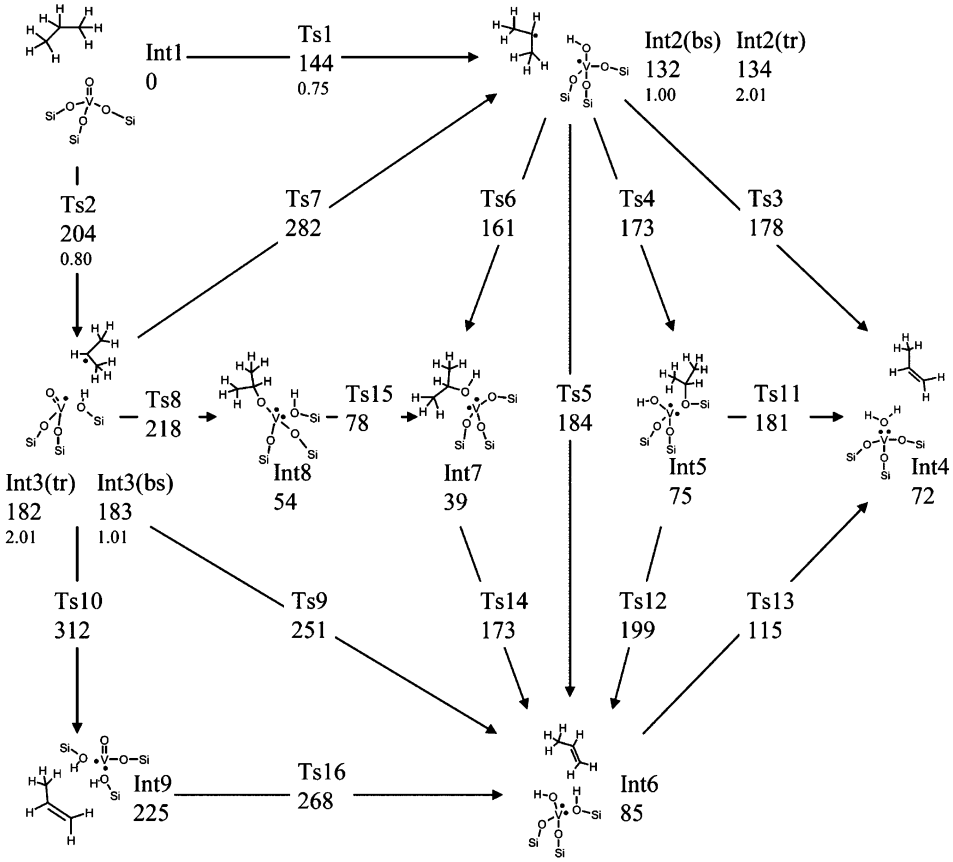

Figure 1. Reaction network of the oxidative dehydrogenation of propane by vanadyl-exchanged silsesquioxane. Values are zero-point energy (in kJ/mol). $\langle S^2 \rangle$ of the open-shell singlets are indicated. All systems except Int1, Ts1, Ts2, Int2(bs), and Int3(bs) are triplet.

of broken-symmetry solutions was also examined. It was indeed possible to localize broken-symmetry transition structures, but they all had higher energies than the corresponding triplet transition structures, usually around 60 kJ/mol after spin-projection. Vanadium is in a $V^{III}(d^2)$ triplet state in all the intermediates and products reached after the transition structures from Int2 and Int3. Crossing from the singlet potential energy surface to the triplet surface occurs in the region of the biradical intermediates Int2 and Int3, where the two surfaces are largely parallel over an extended range and only a few kilojoules per mole apart from each other.[33]

We consider first the reaction pathways from Int2 toward propene formation. A second hydrogen abstraction from a CH_3 group of $C_3H_7^\bullet$ via Ts3 or Ts5 leads directly to propene. The route via Ts3 yields water attached to a $V^{III}(O-)_3$ site. The route via Ts5 leaves the abstracted hydrogen on the oxygen atom of a V−O−Si group and the V−O bond opens. The energies of Ts3 and Ts5 are 178 and 184 kJ/mol, respectively. The propyl radical can also rebind to an oxygen atom of the $HOV^{IV}(O-)_3$ surface site, either to the V−O−Si bond via Ts4 or to the VOH bond via Ts6. With +173 and +161 kJ/mol Ts4 and Ts6 respectively are lower than both Ts3 and Ts5. The route through Ts6 is kinetically dominant whatever the temperature.

From Int4, which is reached after Ts3, desorption of propene costs 23 kJ/mol (Int10+propene), and the water binding to the $V^{III}(O-)_3$ site is 86 kJ/mol. The energy of Int4 is +72 kJ/mol with respect to Int1. The exothermic conversion of propane and oxygen to propene and water is not sufficient to compensate for the endothermic conversion of V^V to V^{III} and oxygen.[25] The energy of the alkoxy species Int5 that is reached after Ts4 is only 3 kJ/mol higher than that of Int4. However, its free energy increases more strongly with increasing temperature due to its more constrained structure. Removal of propene from Int6 that is reached after Ts5 requires only 15 kJ/mol. When temperature increases, the free energy of this complex increases similarly to that of Int4. Among the intermediates attainable from Int2, Int7 that is reached via Ts6 has the lowest energy. Its structure corresponds to isopropyl alcohol attached to the $V^{III}(O-)_3$ site. The interaction energy of isopropyl alcohol with $V^{III}(O-)_3$ is 102 kJ/mol, comparable with the interaction between water and the $V^{III}(O-)_3$ site in Int10. The OH stretching vibration frequencies of isopropyl alcohol when adsorbed onto the V^{III}-$(O-)_3$ site and when in gas phase are 3724 and 3807 cm^{-1}, respectively. Apart from Int1, this intermediate has the lowest energy in the whole reaction network. Only at high temperature does its free energy become more positive than that of the product Int4.

We consider now the reaction pathways from Int3 toward propene. Int6 and Int7 can also be reached from Int3 through two-step mechanisms with prohibitively high barriers. Int2 and Int3 are connected by the high-energy transition structure Ts7. The energies of Ts7 and Int3 relative to Int2 are little affected by the interaction of the propyl radical with the surface model. When we optimize Int2, Ts7, and Int3 in the absence of the propyl radical, we find that the surface models in the doublet state of Ts7 and Int3 are 143 and 60 kJ/mol, respectively, above that of Int2.

From Int3 two reaction routes yield propene by abstraction of a second hydrogen atom from the propyl radical. Int6 is reached when hydrogen is transferred to the vanadyl oxygen atom via Ts9. The energy of Ts9 is +251 kJ/mol with respect to Int1. Hydrogen transfer to the oxygen atom in one of the two V−O−Si bonds yields the high-energy intermediate Int9 via a prohibitively high barrier (Ts10). The alkoxy species Int8

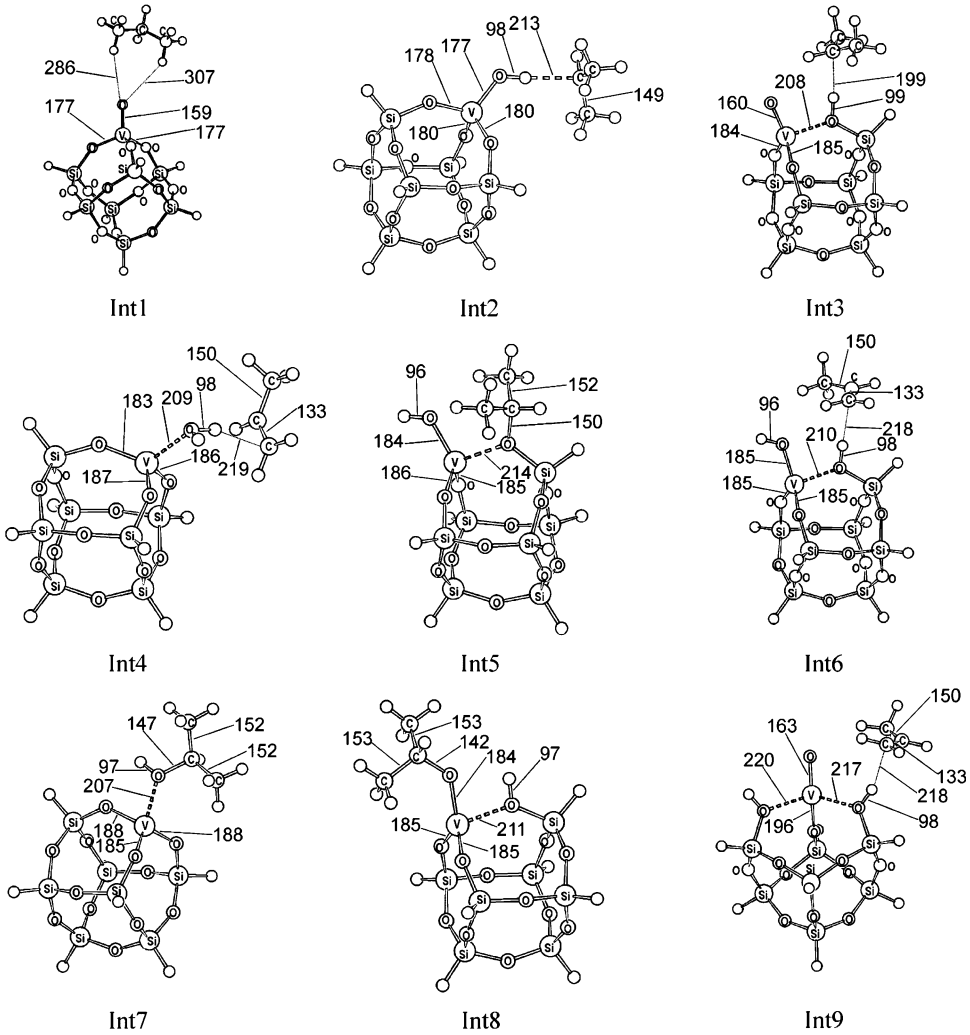

Figure 2. Stable structures of different pathways for the oxidative dehydrogenation of propane. The labels are the same as in Figure 1. The distances are in picometers.

that is reached from Int3 through Ts8 is rather stable. Ts8 has a rather high energy, but it is the lowest one from Int3 toward propene formation at any temperature.

All reaction intermediates in the oxidative dehydrogenation of propane by $O{=}V(OSi)_3$ sites are described now, but there are two additional groups of transition structures. Ts11, Ts12, and Ts14 are transition structures that lead to propene from alkoxide or alcohol. Ts13, Ts15, and Ts16 are transition structures for hydrogen exchange between oxygen atoms.

In Int5, a hydrogen atom of one of the CH_3 groups can jump to an oxygen atom of the surface yielding propene in two ways. Water can be formed through Ts11 (+181 kJ/mol), or a bridging hydroxyl (Int6) can be formed via Ts12, which is 18 kJ/mol above Ts11. The free energy difference between Ts11 and Ts12 increases with temperature. From Int7, only one transition structure leading to propene was found. Ts14 links Int7 to Int6 (+173 kJ/mol). A transition structure corresponding to the elimination of water from isopropyl alcohol (connecting Int4 and Int7) "collapses" to a transition structure similar to Ts3.

The second group of transition structures connects Int6 to Int4, Int8 to Int7, and Int9 to Int6. A hydrogen atom attached to oxygen in a V−O−Si bridge jumps to the oxygen atom originating from the vanadyl group (see Ts13, Ts15, and Ts16). Ts13 has a much lower energy than any other transition structure accessible from Int6, and a fast conversion of Int6 into Int4 occurs. This remains valid when temperature is considered. Ts15, which connects the two reaction intermediates of lowest energy, namely Int8 and Int7, has the lowest energy of all transition structures.

3.2. Cooperating Monomeric Sites. The mechanism described so far proceeds via a diradical intermediate in two subsequent hydrogen abstraction steps of which the second has signifcantly higher barriers. Monomeric vanadium oxide sites can be more active if the second hydrogen abstraction occurs on a different, "unreacted", monomeric vanadia site. In this case, two $HO{-}V^{IV}(d^1)$ species are reached at the end of the reaction instead of one $H_2O{\cdot}V^{III}(d^2)$ species. The dominant reaction pathways for this situation are shown in Figure 4, and the energies are reported in Table 2. Details of the structures can be found in Figures 5 and 6.

Once the intermediate Int2 is formed, the propyl radical may desorb from the $HOV^{IV}(d^1)$ site and re-adsorb to an unreacted $O{=}V^{V}(d^0)$ species elsewhere (Int13). Diffusion on the surface is also possible instead of desorption/readsorption steps. Table 2 shows that $C_3H_7^{\bullet}$ desorption is thermodynamically feasible at reaction temperature, and the free energy of $Int12{+}C_3H_7^{\bullet}$ is lower than the free energies of Ts2 and Ts17. This also remains true if the increment of 37 ± 5 kJ/mol[31] mentioned above is added to the energy of $Int12{+}C_3H_7^{\bullet}$ to correct for missing dispersion contributions. After $C_3H_7^{\bullet}$ has re-adsorbed to an unreacted active $O{=}V(O{-})_3$ site (Int13), the latter abstracts another hydrogen atom yielding C_3H_6. As we saw before, the

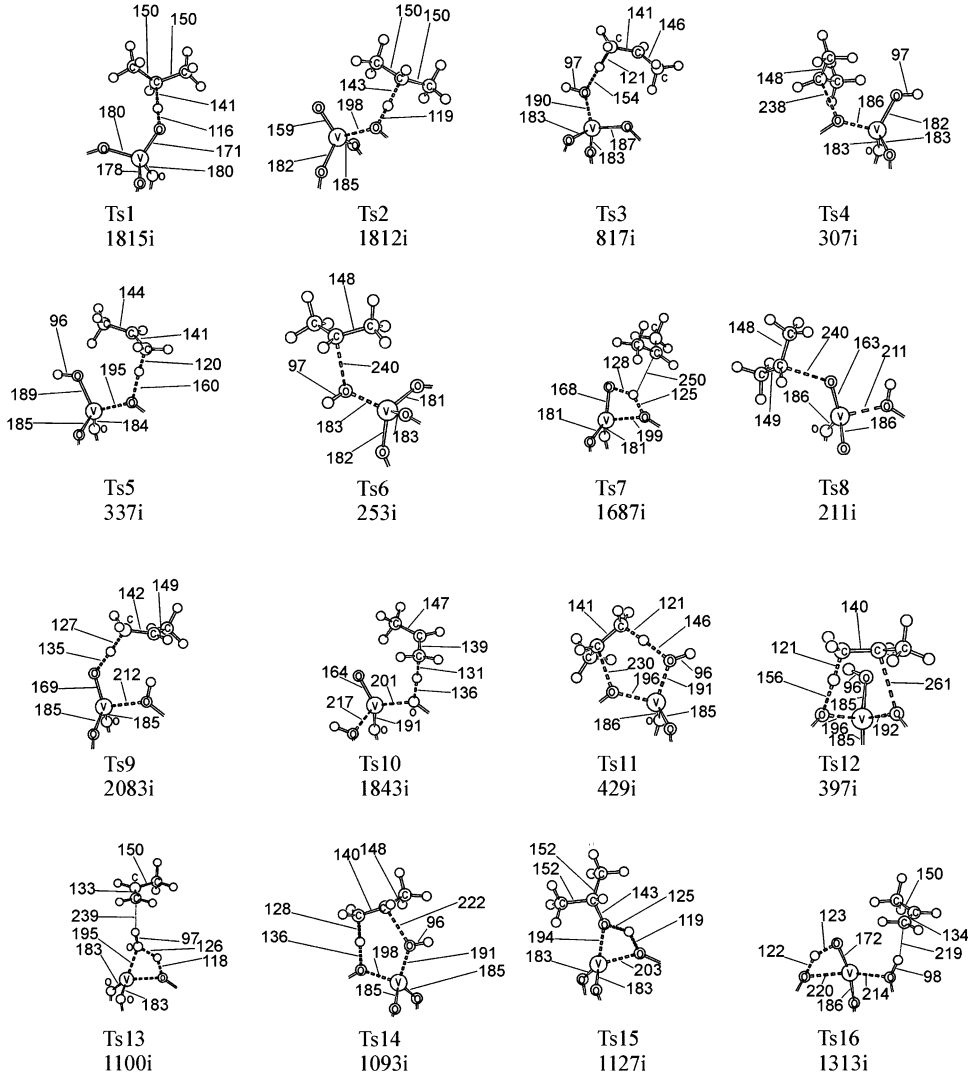

Figure 3. Transition structures of the ODH of propane. The labels are the same as in Figure 1. The distances are in picometers. The broken lines indicate the bonds that are being formed or broken in the transition mode. The imaginary frequencies belonging to these modes are also given (in cm^{-1}).

vanadyl oxygen atom is much more active than a bridging V−O−Si oxygen site, and we can safely consider only two reaction routes. In the first, C_3H_6 is formed in a single step (Int14) by hydrogen abstraction from $C_3H_7^{\bullet}$ (Ts17). In the second, $C_3H_7^{\bullet}$ attaches to the vanadyl oxygen atom (Ts18), forming isopropoxide (Int15). $V^V(d^0)$ is reduced to $V^{IV}(d^1)$ in both cases.

Energy barriers and reaction energies for the second hydrogen abstraction are all lower if it occurs on an "unrecated" $O{=}V^V$ site instead of a $HO{-}V^{IV}$ site. Ts17 is the analogue of Ts3, except that two $V^{IV}(d^1)$ species are reached in the former case, and a $V^{III}(d^2)$ species in the latter case. The energy is only 6 kJ/mol lower for Ts17 than for Ts3, but the free energy difference between the two transition structures increases with temperature and reaches 22 kJ/mol at 800 K. The same trend applies to Ts18 and Ts6, which are the transition structures for formation of surface propoxides. The energy and free energy differences are 10 and 23 kJ/mol at 0 and 800 K, respectively. The products are around 30 kJ/mol more stable when two $HO{-}V^{IV}(d^1)$ are reached (Int14 and Int15) instead of $H_2O{\cdot}V^{III}(d^2)$. The free energy increases with temperature are equivalent for the intermediates Int4-Int14 and Int7-Int15. The same holds after C_3H_6 has desorbed.

3.3. Heterolytic Bond Dissociation. It was suggested that oxidative dehydrogenation can be achieved through heterolytic bond dissociation (CH addition on the V═O bond).[6,32] We investigated the closed-shell singlet reaction pathways (Figure 7) and found that the reaction intermediates and transition structures have significantly higher energies than for the open-shell singlet reaction pathways. This was also found before by Fu et al.[7] for the reaction of propane with the Mo_3O_9 cluster. The closed and open-shell potential energy surfaces never intersect. Therefore, spin-crossover as described[10,11] for propane dehydrogenation by VO_2^+ or $V_3O_7^+$ does not occur. This is one of many reactivity differences between charged vanadium oxide species in the gas phase and neutral vanadium oxide species on surfaces. Another critical difference is that the oxidation part of the catalytic cycle, that is, formation of propene and $H_2O{\cdot}V^{III}(d^2)$, is endothermic for the surface species studied here (Table 1), whereas it is strongly exothermic with VO_2^+. The energy of $C_3H_6{\cdot}VO_2H_2^+$ is −347 kJ/mol with respect to $C_3H_8{\cdot}VO_2^+$.[10] The corresponding difference for the $O{=}V(O{-})_3$ surface site, that is, the energy difference between Int4 and Int1, is +74 kJ/mol. This difference in reaction energies is in agreement with the difference in oxygen defect formation energies between charged gas phase and neutral vanadium oxide

TABLE 1: Electronic and Zero-Point Energies and Gibbs Free Energies of the Intermediates and Transition States in the Oxidative Dehydrogenation of Propane[a]

			G_T		
structure	E_{el}	E_{ZP}	200	600	800
Int0+propane[b]	0	0	0	0	0
Int1	−1	0	19	49	62
Ts1	163 (136)	144 (117)	172 (145)	224 (197)	247 (220)
Ts2	224 (211)	204 (191)	240 (227)	312 (299)	345 (332)
Int2(bs)	143 (142)	133 (132)	154 (153)	185 (184)	197 (196)
Int2(tr)	144	134	158	195	210
Int3(bs)	192 (192)	182 (182)	206 (206)	241 (241)	256 (256)
Int3(tr)	192	183	207	243	258
Ts3	198	178	207	258	280
Ts4	184	173	204	259	284
Ts5	204	184	212	263	286
Ts6	172	161	188	233	253
Ts7	307	283	305	337	351
Ts8	230	218	244	284	301
Ts9	274	251	282	339	366
Ts10	334	312	342	373	414
Int4	76	72	96	131	145
Int5	72	75	109	171	200
Int6	91	84	111	150	166
Int7	32	39	68	123	149
Int8	51	53	84	139	165
Int9	232	225	250	285	299
Ts11	194	181	214	276	304
Ts12	215	199	236	311	346
Ts13	131	115	139	177	193
Ts14	188	173	205	264	291
Ts15	84	77	109	171	200
Ts16	286	268	295	339	358
Int10+propene[b]	102	94	90	72	62
Int11+H_2O+propene	198	180	151	79	42
Int11+isopropyl alcohol	141	142	139	131	127

[a] E_{el}, E_{ZPE}, and G_T are electronic energy, zero-point energy, and Gibbs free energy at standard pressure, respectively, in kJ/mol. The temperature is in K. The numbers in parentheses are spin-projected energies. [b] To get an estimate of the van der Waals contribution to the reaction, the energies of Int0+propane, Int10+propene, Int11+H_2O+propene, and Int11+isopropyl alcohol can be increased by 37 ± 5 kJ/mol.[31]

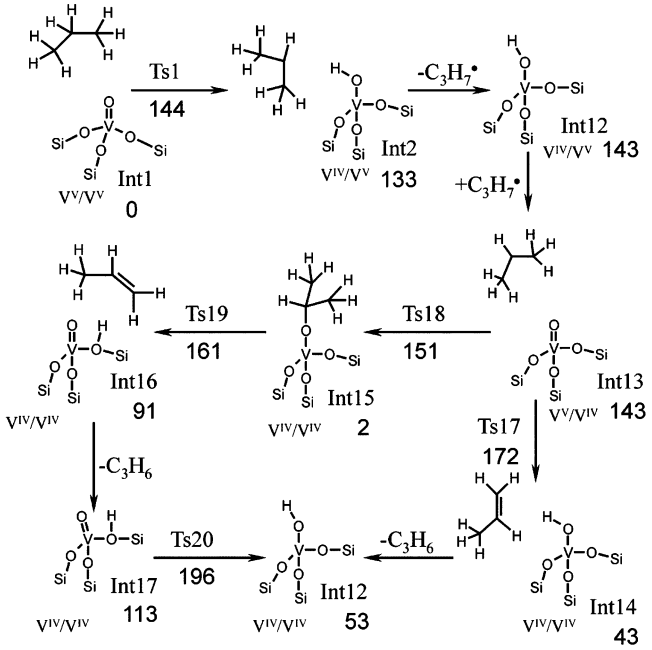

Figure 4. Reaction pathways in the ODH of propane by two cooperating active sites. V^X/V^Y indicates the oxidation states X and Y of the two sites. The numbers are zero-point energies (in kJ/mol).

species on the surface.[25] In propane dehydrogenation by $V_3O_7^+$, the barrier for the CH addition onto the V=O bond is only marginally higher than the barrier for the first hydrogen atom abstraction from propane, which is the rate-determining step.[10,11]

4. Discussion

4.1. Comparison with Calculations for Bulk V_2O_5 Surfaces. Very recently, Fu et al.[9] studied oxidative dehydrogenation of propane on single-crystal V_2O_5(001) surfaces, which also exhibit vanadyl (O=V) sites, albeit in a different environment. At these sites propene can be formed by a two-step hydrogen-abstraction mechanism leading to surface propoxy species similar to Int8. The barriers for the two steps are about the same, of the order of 110 kJ/mol. The propoxy species can also be reached with similar barriers by inserting the vanadyl oxygen into the C−H bond of propane. Bridging V−O−V sites which are also present on the V_2O_5(001) crystal surface have also been found active in propane ODH (oxo-insertion mechanism).[9]

Unfortunately, the density functional used in ref 9 (PW91) was different from the one we use (B3LYP). B3LYP was applied in a study of propane ODH on cluster models of the V_2O_5(001) crystal surface,[8b] but since broken-symmetry solutions were not considered the H-abstraction mechanism was not found in ref 8b and much too high barriers were obtained for the oxo-insertion mechanism. PBE (which yields virtually the same results as PW91) has been found to yield larger energies for oxygen defect formation of vanadia (both supported and crystalline),[25] and test calculations for Ts3 showed that PBE barriers can be higher than B3LYP barriers for propene formation on supported vanadia species. This implies that sites on V_2O_5(001) crystal surfaces could be significantly more active in the ODH of propane than monomeric vanadia species on silica support. The smaller apparent turnover frequencies observed for VO_x/SiO_2 and VO_x/Al_2O_3 catalysts[37,41] at vanadia loadings high enough that V_2O_5 crystallites are present (above 8 V/nm^2)

TABLE 2: Electronic and Zero-Point Energies and Gibbs Free Energies of the Intermediates and Transition States in the Oxidative Dehydrogenation of Propane[a]

			G_T		
structure	E_{el}	E_{ZP}	200	600	800
Int0+Int0+propane[b]	0	0	0	0	0
Int0+Int2(bs)	143 (142)	133 (132)	154 (153)	185 (184)	197 (196)
Int0+Int2(tr)	144	134	158	195	210
Int0+Int12+$C_3H_7^{\bullet}$ [b]	160	143	141	125	115
Int12+Int13	158	143	154	157	155
Int12+Ts17	196	172	199	240	258
Int12+Ts18	165	151	174	208	222
Int12+Int14	53	43	69	107	122
Int12+Int15	2	2	27	70	89
Int12+Ts19	179	161	192	250	276
Int12+Int16	100	91	116	152	166
Int12+Int17+propene[b]	126	113	109	91	79
Int12+Ts20+propene[b]	221	196	192	178	170
2 Int12+propene[b]	67	53	51	36	27

[a] E_{el}, E_{ZPE}, and G_T are electronic energy, zero-point energy, and Gibbs free energy at standard pressure, respectively, in kJ/mol. The temperature is in K. The numbers in parentheses are spin-projected energies. [b] To get an estimate of the van der Waals contribution to the reaction, the energies of 2 Int0+propane, Int0+Int12+$C_3H_7^{\bullet}$, Int12+Int17+propene, Int12+Ts20+propene, and 2 Int12+propene can be increased by 37 ± 5 kJ/mol.[31]

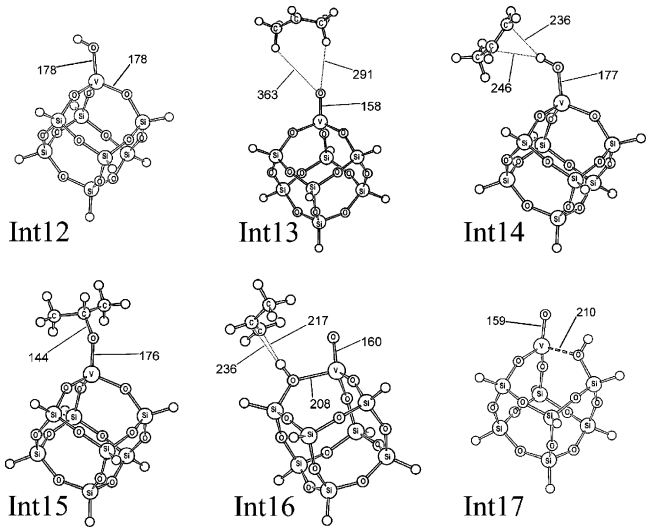

Figure 5. Geometry details of the reaction intermediates in the ODH of propane by cooperative monomeric vanadia sites (see Figure 4). The distances are in picometers.

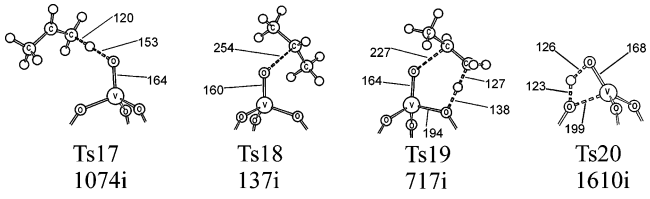

Figure 6. Transition structures of the ODH of propane by cooperative monomeric site. The labels are the same as in Figure 4. The distances are in picometers. The broken lines indicate the bonds that are being formed or broken in the transition mode. The imaginary frequencies belonging to these modes are also given (in cm^{-1}).

are not in contradiction. The majority of vanadia sites are inside the bulk of V_2O_5 crystallites and not accessible in such three-dimensional vanadia particles.

4.2. Kinetic Considerations. Hydrogen abstraction by the vanadyl oxygen atom is the initial step in the oxidative dehydrogenation of propane by supported vanadium oxide species. The diradical intermediate that is reached via the diradicaloid transition structure Ts1 consists of a propyl radical attached to a $HO-V(O-)_3$ site and has similar energies in the singlet and triplet states (Int2). Spin-crossing to the triplet state most likely occurs in this step. For the second hydrogen

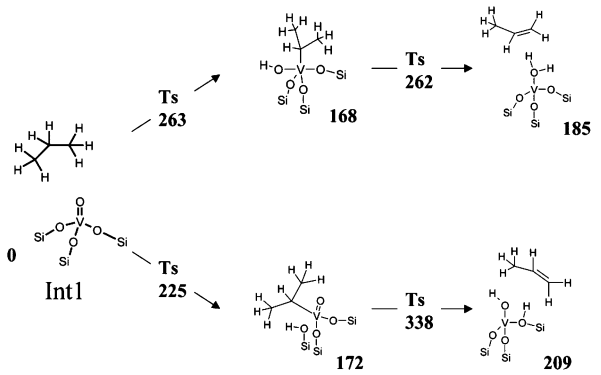

Figure 7. Reaction pathways and zero-point energies (in kJ/mol) for ODH by C−H addition on the O═V bond (singlet closed-shell electronic structure).

abstraction there are many possible pathways that lead to propene formation. First, we consider cases in which the second hydrogen abstraction occurs at the same site as the first one, yielding a $H_2O{\cdot}V^{III}(O-)_3$ site (Figure 1). To ease the discussion, we consider the most significant reaction intermediates and calculate from the data in Table 1 the rates relative to the fastest route using classical transition state theory (eq 7).

$$r_x/r_y = \exp(-\Delta G_{Ts}/RT) = \exp((-G_{Ts1} + G_{Ts2})/RT) \quad (7)$$

Table 3 shows the results. For instance, Ts3, Ts4, Ts5, Ts6, and Ts7 can be crossed from Int2. Instead of giving all reaction rates, only the ratios are given for Ts3, Ts4, Ts5, and Ts7 with respect to the fastest route, Ts6. The only product that can be formed at low temperature from Int2 is Int7 through Ts6. With increasing temperature, the relative rates for conversion of Int2 through Ts3, Ts4, and Ts5 become larger (Table 3). The only route that can be excluded at all temperatures is the one through Ts7. Conversion between Int7 and Int8 is many orders of magnitude faster than the other routes from these intermediates. Int7 and Int8 can then be considered to be permanently at equilibrium. Because Int8 is the less stable among them, it is not further considered. From Int6, the conversion into Int4 via Ts13 is also many orders of magnitude faster than the other reactions, and, therefore, Int6 does not need to be considered as a separate species. This way it is possible to simplify the reaction network for the oxidative dehydrogenation of propane as shown in Figure 8. Surface alcohol and alkoxy species such

TABLE 3: Most Favorable Kinetic Routes from the Different Reaction Intermediates in the Oxidative Dehydrogenation of Propane by an Isolated Site as a Function of Temperature (K)

structure[a]	ratio of reaction rates[b]	T 200	T 600	T 800
Int2	r_3/r_6	1×10^{-5}	8×10^{-3}	2×10^{-2}
	r_4/r_6	6×10^{-5}	6×10^{-3}	1×10^{-2}
	r_5/r_6	4×10^{-7}	3×10^{-3}	8×10^{-3}
	r_7/r_6	3×10^{-31}	9×10^{-10}	4×10^{-7}
Int5	r_{11}/r_4	3×10^{-3}	3×10^{-2}	4×10^{-2}
	r_{12}/r_4	5×10^{-9}	3×10^{-5}	8×10^{-5}
Int6	r_5/r_{13}	6×10^{-20}	3×10^{-8}	9×10^{-7}
	r_{12}/r_{13}	4×10^{-26}	2×10^{-12}	1×10^{-10}
	r_{14}/r_{13}	6×10^{-18}	3×10^{-8}	4×10^{-7}
	r_{16}/r_{13}	2×10^{-41}	8×10^{-15}	2×10^{-11}
Int7	r_6/r_{15}	2×10^{-21}	3×10^{-6}	3×10^{-4}
	r_{14}/r_{15}	9×10^{-26}	7×10^{-9}	1×10^{-6}
Int8	r_8/r_{15}	5×10^{-36}	1×10^{-10}	3×10^{-7}

[a] The labels used to designate the structures are the same as in Figure 1. [b] See eq 7 and Table 1 for the values of the Gibbs free energies. The labels are the same as in Figure 1.

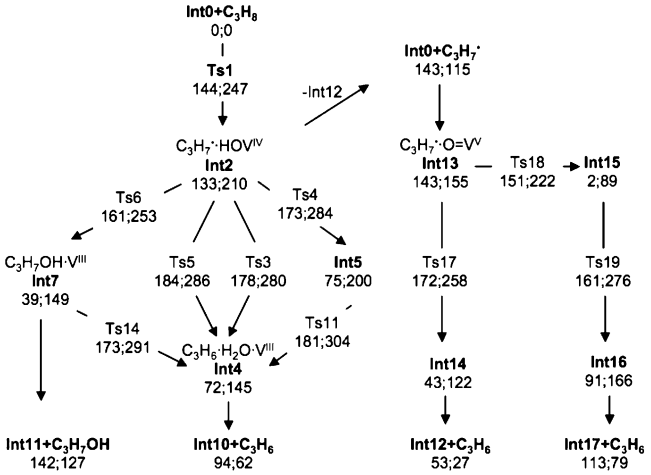

Figure 8. The dominant reaction pathways in oxidative propane dehydrogenation on vanadia sites. The numbers are zero-point energies and Gibbs free energies at 800 K (in kJ/mol).

as Int7 and Int5 constitute the predominant reaction intermediates at low temperature. At reaction temperatures, that is, above 600 K, the alkoxy species Int5 becomes less stable than the product, Int4.

Propene can be formed via Ts3 or Ts5, or from Int5 via Ts11 and from Int7 via Ts14. All four of these routes for the second hydrogen abstraction are included, because their energies are too close to favor one over the other. While the route from Int7 via Ts14 dominates at low temperature, at higher temperatures it is the conversion via Ts3, closely followed by the conversions through Ts5 and Ts14. To get apparent zero-point energy and Gibbs free energy barriers from the B3LYP data in Table 1 we need realistic values for the energy of adsorption of propane onto the catalyst surface. We add the experimental value for propane adsorption onto crystalline V_2O_5 (37 ± 5 kJ/mol)[31] to all intermediates with hydrocarbon species desorbed from the surface. Table 4 shows the corresponding apparent reaction rate constants for different routes of the second hydrogen abstraction. At high temperature (800 K), direct propene formation through Ts3 is around 2 and 5 times faster than that through Ts5 and Ts4, respectively, and 37 times faster than that through Ts11.

So far, we did not consider desorption of surface hydrocarbon species into the gas phase, which is favored by entropy, and readsorption onto other active sites on the surface. Desorption of isopropyl alcohol from Int7 yielding Int11+isopropyl alcohol requires 103 kJ/mol, but the Gibbs free energy change is −22 kJ/mol at 800 K (Figure 8, Table 1). Desorption of the propyl radical from Int2 yielding Int12+$C_3H_7^\bullet$ requires 10 kJ/mol only, while the Gibbs free energy change is −95 kJ/mol at 800 K. Desorbed isopropyl alcohol could be dehydrated on acidic sites of the support.[34−36] The apparent activation energy of isopropyl alcohol dehydration to propene is around 125 and 113 ± 3 kJ/mol when catalyzed by silica and alumina, respectively. Desorbed isopropyl alcohol could also re-adsorb at an "unreacted" O═V(O−)$_3$ site and undergo further oxidation to ketone, eventually leading to total oxidation of the alkane to CO_x and water.[1,2,6] Apparent zero-point energy barriers for oxidation of alcohols to aldehydes (or ketones) are about 98 kJ/mol (intrinsic B3LYP barrier of 114 kJ/mol plus CCSD(T) decrement of 17 kJ/mol).[16] However, when desorption of the propyl radical from Int2 is also considered, the fraction of isopropyl alcohol formed via Ts6 from Int2 is tiny compared to the amount of propene formed via Int13 and Ts 17 (see below), and the path toward higher oxidized products most likely goes through propene.

The following kinetic scheme takes desorption of the propyl radical from Int2 leaving an Int12 site (V^{IV}) into account (k_1),

$$\text{Int0} + \text{C}_3\text{H}_8 \underset{k_{-1}}{\overset{k_1}{\rightleftharpoons}} \text{Int12} + \text{C}_3\text{H}_7^\bullet$$

$$\text{Int0} + \text{C}_3\text{H}_7^\bullet \xrightarrow{k_2} \text{Int12} + \text{C}_3\text{H}_6$$

$$\text{Int12} + \text{C}_3\text{H}_7^\bullet \xrightarrow{k_3} \text{Int11} + \text{C}_3\text{H}_7\text{OH} \qquad (8)$$

Readsorption can occur on the same type of site Int12, yielding either propane back via Ts1 (k_{-1}) or leading to isopropyl alcohol via Ts6 (k_2), but readsorption can also occur at an "unreacted" Int0 site yielding propene via Ts17 or Ts19 (k_3).

For a stationary concentration of propyl radicals in the gas phase, and if we further assume (in accord with the Mars−van Krevelen mechanism) that the fraction of active sites that are in the reduced state is small, [Int12]/[Int0] ≪ 1, the expression for the rate of propene formation becomes

TABLE 4: Apparent Zero-Point Energy Barriers (kJ/mol) and Apparent Rate Constants[a] (s^{-1}) at Different Temperatures (K) for Key Reaction Steps[a]

step	$E_{ZP}^{Ts} - E_{ZP}^{S+hc}$	$k_{app}(200)$	$k_{app}(600)$	$k_{app}(800)$
Ts1	107	$6.3 \times 10^{-23}(5.5 \times 10^5)$	$1.7 \times 10^{-3}(3.7 \times 10^6)$	$8.8 \times 10^{-1}(8.5 \times 10^6)$
Ts3	141	$4.5 \times 10^{-32}(3.0 \times 10^5)$	$2.0 \times 10^{-6}(3.7 \times 10^6)$	$6.2 \times 10^{-3}(9.9 \times 10^6)$
Ts5	147	$2.2 \times 10^{-33}(5.5 \times 10^5)$	$7.2 \times 10^{-7}(4.5 \times 10^6)$	$2.5 \times 10^{-3}(9.9 \times 10^6)$
Ts14	136	$1.5 \times 10^{-31}(5.0 \times 10^4)$	$5.9 \times 10^{-7}(4.1 \times 10^5)$	$1.2 \times 10^{-3}(9.0 \times 10^5)$
Ts11	144	$6.7 \times 10^{-34}(2.7 \times 10^4)$	$5.3 \times 10^{-8}(1.8 \times 10^5)$	$1.7 \times 10^{-4}(4.2 \times 10^5)$

[a] See eq 6b, the pre-exponential, $(k_B T/h)(q_{Ts}\cdot e/q_S\cdot q_{hc})$, is given in parentheses.

$$\frac{d[C_3H_6]}{dt} = \frac{k_1 k_2 [Int0][C_3H_8]}{(k_{-1} + k_3)[Int12]/[Int0] + k_2} \approx k_1[Int0][C_3H_8] \quad (9)$$

This shows that under such conditions step 1 is rate determining. The apparent rate for the first hydrogen abstraction is included in Table 4.

The rate of propyl alcohol formation relative to the rate of propene formation is proportional to the concentration of reduced sites Int12 relative to the concentration of non-reduced sites Int0.

$$\frac{d[C_3H_7OH]/dt}{d[C_3H_6]/dt} = \frac{k_3}{k_2}\frac{[Int12]}{[Int0]} \ll 1 \quad (10)$$

Since the latter is very small and k_3 and k_2 are comparable, only a tiny fraction of isopropyl alcohol is formed.

In summary, the surface propyl radical is the central intermediate and its formation is the rate-determing step (Ts1). Desorption of propyl radicals leads to a stationary concentration of propyl in the gas phase and leaves reduced $HO-V^{IV}$ sites (Int12) on the surface. Due to fast reoxidation their concentration is much smaller than the concentration of $O{=}V^{V}$ sites (Int0). Therefore the rate of propene formation after readsorption on $O{=}V^{V}$ sites (Ts17) is much larger than the rate for isopropyl alcohol (or propene) formation after readsorption on $HO-V^{IV}$ sites via Ts6 (or Ts3). Going beyond these qualitative considerations requires a microkinetic modeling of a reaction network such as shown in Figure 8. Numerical solutions will be obtained for realistic conditions such as temperature, loading of the catalyst surface with active species, and partial pressure of propane. This will be done in a future publication that also considers larger vanadia species.[43]

4.3. Comparison with Experimental Data. For V_2O_5/SiO_2 catalysts with vanadium surface coverages below 3 V/nm^2 (i.e., below the limit at which V_2O_5 crystallites start to appear) turnover frequencies (TOF) of around 0.01 s^{-1} (748 K)[37] and 0.3×10^{-3} s^{-1} (623 K)[38] have been observed for propene formation. The calculated apparent rate constants for the first hydrogen abstraction (Ts1) are 0.26 s^{-1} at 750 K and 1.7×10^{-3} s^{-1} at 600 K (Table 4), that is, they are about 26 times (750 K) and 5 times (600 K) larger than the experimental numbers. For V_2O_5/SiO_2 catalysts with vanadium surface coverages below 0.5 V/nm^2 (MCM-41), apparent activation energies of 122 ± 20 kJ/mol have been measured for propene formation,[37,39] while values of 101 ± 15 and 112 ± 15 kJ/mol have been obtained for butane conversion.[40] For V_2O_5/Al_2O_3 and V_2O_5/ZrO_2 catalysts the apparent activation energies for propene formation are between 120 and 110 kJ/mol[41] and around 99 kJ/mol,[42] respectively. The upper limit estimate from the calculations for 750 K, $E_a(T) = (H_{Ts} - H_{S+hc}) + RT = 123 \pm 5$ kJ/mol for the first hydrogen abstraction, which includes the ± 5 kJ/mol uncertainty of the experimental adsorption energy,[31] but not the DFT uncertainty, is close to the most directly related experimental value of 122 ± 20 kJ/mol.[37,39]

Comparison of both TOF and activation energies shows that the mechanistic details we suggest are compatible with known observations.

5. Conclusions

We analyzed possible reaction mechanisms for the oxidative dehydrogenation of propane by monomeric vanadium oxide species on silica. The initial step is hydrogen abstraction from propane by the vanadyl oxygen atom leading to a diradical intermediate, namely, $C_3H_7^{\bullet}\cdot HO-V^{IV}(O-)_3$. The corresponding transition state is only found by broken-symmetry calculations. All reaction steps after the first hydrogen atom abstraction that occur at the same active site proceed on the triplet potential energy surface.

Desorption of propyl radicals leads to a stationary concentration of propyl in the gas phase and leaves reduced $HO-V^{IV}(O-)_3$ sites on the surface. Due to fast reoxidation the concentration of the latter is much smaller than the concentration of regenerated (or unreacted) $O{=}V^{V}(O-)_3$ sites. This has two consequences: (i) The rate of propene formation after readsorption on $O{=}V^{V}(O-)_3$ sites is much larger than the rate for isopropyl alcohol (or propene) formation after readsorption on $HO-V^{IV}(O-)_3$ sites. (ii) Formation of propyl radicals by the first hydrogen abstraction from propene becomes rate-limiting. The mechanism suggested is compatible with turnover frequencies and activation energies available, while other suggestions (C−H addition onto the metal oxo bond)[6,32] are not supported by the calculations.

With regard to the type of active oxygen species in the reaction, we find that only vanadyl sites are involved in the rate-determining step, but the second hydrogen abstraction may occur also at V−O−Si bridging oxygen sites without changing the overall kinetics of the reaction.

Comparison with recent DFT calculations for $V_2O_5(001)$ crystal surfaces[9] indicates that vanadia sites may be significantly more active in the ODH of propane if they are part of the bulk surface and not supported as monomers on silica. However, apparent turnover frequencies may be lower for V_2O_5 crystallites on the surface because only a fraction of sites is accessible in three-dimensional particles.

The detailed mechanism presented in this study is a firm basis for future analysis of different kinds of experiments and will be used in microkinetic models. Further work should address the selectivity problem.

Acknowledgment. This work has been supported by Deutsche Forschungsgemeinschaft (Sonderforschungbereich 546) and by an Alexander von Humboldt fellowship for X.R. We thank E. V. Kondratenko (Berlin) for discussions and for making available data on the activation of propane by V_2O_5/SiO_2 prior publication.

References and Notes

(1) Cullis, C. F. *Ind. Eng. Chem.* **1967**, *59*, 19−27.
(2) Batiot, C.; Hodnett, B. K. *Appl. Catal. A* **1996**, *137*, 179−191.
(3) Shaik, S.; De Visser, S. P.; Ogliaro, F.; Schwarz, H.; Schröder, D. *Curr. Opin. Chem. Biol.* **2002**, *6*, 556−567.
(4) Limberg, C. *Angew. Chem., Int. Ed.* **2003**, *42*, 5932−5954.
(5) Chaar, M. A.; Patel, D.; Kung, M. C.; Kung, H. H. *J. Catal.* **1987**, *105*, 483−498.
(6) (a) Blasco, T.; López Nieto, J. M. *Appl. Catal. A* **1997**, *157*, 117−142. (b) Blasco, T.; López Nieto, J. M.; Dejoz, A.; Vázquez, M. I. *J. Catal.* **1995**, *157*, 271−282.
(7) Fu, G.; Xu, X.; Lu, X.; Wan, H. *J. Phys. Chem. B* **2005**, *109*, 6416−6421.
(8) (a) Gilardoni, F.; Bell, A. T.; Chakraborty, A.; Boulet, P. *J. Phys. Chem. B* **2000**, *104*, 12250−12255. (b) Redfern, P. C.; Zapol, P.; Sternberg, M.; Adiga, S. P.; Zygmunt, S. A.; Curtiss, L. A. *J. Phys. Chem. B* **2006**, *110*, 8363−8371.
(9) Fu, H.; Liu, Z.-P.; Li, Z.-H.; Wang, W.-N.; Fan, K.-N. *J. Am. Chem. Soc.* **2006**, *128*, 11114−11123.
(10) Engeser, M.; Schlangen, M.; Schröder, D.; Schwarz, H. *Organometallics* **2003**, *22*, 3933−3943.
(11) Feyel, S.; Schröder, D.; Rozanska, X.; Sauer, J.; Schwarz, H. *Angew. Chem., Int. Ed.* **2006**, *45*, 4677−4681.
(12) Khodakov, A.; Olthof, B.; Bell, A. T.; Iglesia, E. *J. Catal.* **1999**, *181*, 205−216.
(13) Weckhuysen, B. M.; Keller, D. E. *Catal. Today* **2003**, *78*, 25−46.

(14) Mars, P.; Van Krevelen, D. W. *Spec. Sup. Chem. Eng. Sci*. **1954**, *3*, 41−57.
(15) Chen, K.; Iglesia, E.; Bell, A. T. *J. Catal*. **2000**, *192*, 197−203.
(16) Döbler, J.; Pritzsche, M.; Sauer, J. *J. Am. Chem. Soc*. **2005**, *127*, 10861−10868.
(17) Magg, N.; Immaraporn, B.; Giorgi, J. B.; Schroeder, T.; Bäumer, M.; Döbler, J.; Wu, Z.; Kondratenko, E.; Cherian, M.; Baerns, M.; Stair, P. C.; Sauer, J.; Freund, H.-J. *J. Catal*. **2004**, *226*, 88−100.
(18) Calzaferri, G.; Hoffmann, R. *J. Chem. Soc. Dalton Trans*. **1991**, 917−928.
(19) Bieniok, A. M.; Bürgi, H.-B. *J. Phys. Chem*. **1994**, *98*, 10735−10741.
(20) Civalleri, B.; Garrone, E.; Ugliengo, P. *Chem. Phys. Lett*. **1998**, *294*, 103.
(21) Sauer, J.; Hill, J.-R. *Chem. Phys. Lett*. **1994**, *218*, 333−337.
(22) (a) Becke, A. D. *J. Chem. Phys*. **1993**, *98*, 5648−5652. (b) Lee, C.; Yang, W.; Parr, R. G. *Phys. Rev. B* **1988**, *37*, 785−789.
(23) Schäfer, A.; Huber, C.; Ahlrichs, R. *J. Chem. Phys*. **1994**, *100*, 5829−5835.
(24) (a) Ahlrichs, R.; Bär, M.; Häser, M.; Horn, H.; Kölmel, C. *Chem. Phys. Lett*. **1989**, *162*, 165−169. (b) Treutler, O.; Ahlrichs, R. *J. Chem. Phys*. **1995**, *102*, 346−354. (c) Deglmann, P.; Furche, F.; Ahlrichs, R. *Chem. Phys. Lett*. **2002**, *362*, 511−518.
(25) Sauer, J.; Döbler, J. *Dalton Trans*. **2004**, 3116−3121.
(26) Noodleman, L. *J. Chem. Phys*. **1981**, *74*, 5737−5743.
(27) Caballol, R.; Castell, O.; Illas, F.; Moreira, I. de P. R.; Malrieu, J. P. *J. Phys. Chem. A* **1997**, *101*, 7860−7866.
(28) Gräfenstein, J.; Hjerpe, A. M.; Kraka, E.; Cremer, D. *J. Phys. Chem. A* **2000**, *104*, 1748−1761.
(29) Wesolowski, T. A.; Parisel, O.; Ellinger, Y.; Weber, J. *J. Phys. Chem. A* **1997**, *101*, 7818−7825.
(30) Grimme, S. *J. Comput. Chem*. **2004**, *25*, 1463−1473.
(31) Kämper, A.; Auroux, A.; Baerns, M. *Phys. Chem. Chem. Phys*. **2000**, *2*, 1069−1075.
(32) Oyama, S. T. *J. Catal*. **1991**, *128*, 210−217.
(33) Carréon-Macedo, J. L.; Harvey, J. N. *J. Am. Chem. Soc*. **2004**, *126*, 5789−5797.
(34) De Mourgues, L.; Peyron, F.; Trambouze, Y.; Prette, M. *J. Catal*. **1967**, *7*, 117−125.
(35) Butler, J. D.; Poles, T. C.; Wood, B. T. *J. Catal*. **1970**, *16*, 239−244.
(36) Knözinger, H.; Bühl, H.; Kochloefl, K. *J. Catal*. **1972**, *24*, 57−68.
(37) Kondratenko, E.; Cherian, M.; Baerns, M.; Su, D.; Schlögl, R.; Wang, X.; Wachs, I. E. *J. Catal*. **2005**, *234*, 131−142.
(38) Tian, H.; Ross, E. I.; Wachs, I. E. *J. Phys. Chem. B* **2006**, *110*, 9593−9600.
(39) Kondratenko, E. V.; Baerns, M. Private communication.
(40) Owens, L.; Kung, H. H. *J. Catal*. **1993**, *144*, 202−213.
(41) Argyle, M. D.; Chen, K.; Bell, A. T.; Iglesia, E. *J. Catal*. **2002**, *208*, 139−149.
(42) Chen, K.; Bell, A. T.; Iglesia, E. *J. Phys. Chem. B* **2000**, *104*, 1292−1299.
(43) Rozanska, X.; Fortrie, R.; Sauer, J. In preparation.